This is an open access article published under a Creative Commons Attribution (CC-BY) License, which permits unrestricted use, distribution and reproduction in any medium, provided the author and source are cited.

analytical chemistry

Article

Cite This: *Anal. Chem.* 2019, 91, 10016−10025

pubs.acs.org/ac

Sequence-Specific Detection of Unlabeled Nucleic Acid Biomarkers Using a "One-Pot" 3D Molecular Sensor

Sameen Yousaf,[†] Patrick J. S. King,[†,§] Aline F. Miller,[‡] Alberto Saiani,[‡] David J. Clarke,[†] Linda T. Trivoluzzi,[†] Harmesh S. Aojula,[†] and Elena V. Bichenkova*[,†]

[†]School of Health Sciences, University of Manchester, Oxford Road, Manchester M13 9PT, U.K.

[‡]Manchester Institute of Biotechnology, 131 Princess Street, Manchester M1 7DN, U.K.

Supporting Information

ABSTRACT: DNA and RNA biomarkers have not progressed beyond the automated specialized clinic due to failure in the reproducibility necessary to standardize robust and rapid nucleic acid detection at the point of care, where health outcomes can be most improved by early-stage diagnosis and precise monitoring of therapy and disease prognosis. We demonstrate here a new analytical platform to meet this challenge using functional 3D hydrogels engineered from peptide and oligonucleotide building blocks to provide sequence-specific, PCR-free fluorescent detection of unlabeled nucleic acid sequences. We discriminated at picomolar detection limits (<7 pM) "perfect-match" from mismatched sequences, down to a single nucleotide mutation, buried within longer lengths of the target. Detailed characterization by NMR, TEM, mass spectrometry, and rheology provided the structural understanding to design these hybrid peptide−oligonucleotide biomaterials with the desired sequence sensitivity and detection limit. We discuss the generic design, which is based on a highly predictable secondary structure of the oligonucleotide components, as a platform to detect genetic abnormalities and to screen for pathogenic conditions at the level of both DNA (e.g., SNPs) and RNA (messenger, micro, and viral genomic RNA).

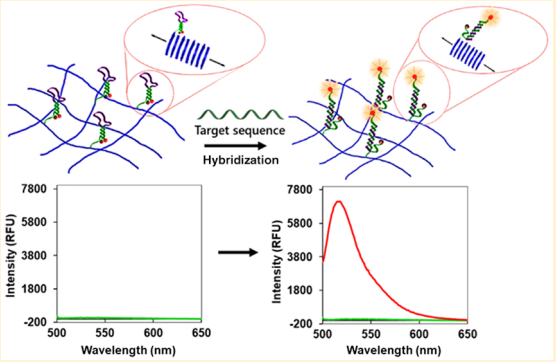

Nucleic acid sequences (DNA and RNA) are well recognized as important diagnostic and prognostic biomarkers for a wide range of pathological conditions in humans. Identification of single or multiple nucleotide polymorphisms at the DNA level can be crucial in recognizing patient susceptibility to most monogenic or complex diseases, such as Bardet−Biedl syndrome,[1] diabetes,[2] rheumatoid arthritis,[3] Alzheimer's disease,[4] sickle-cell anemia,[5] schizophrenia,[6] cancer,[7,8] multiple sclerosis,[9] cystic fibrosis,[10] muscular dystrophy,[11] and Parkinson's disease.[12] Of particular diagnostic importance is the detection of single nucleotide polymorphisms (SNPs), which are often associated with different types of human pathophysiology.[13−16] Similarly of growing importance is the rapid detection of overexpressed functional RNAs (e.g. mRNAs or nonprotein-coding RNAs, including miRNA, siRNA, piRNA, and/or lncRNA), with the advantage of earlier diagnosis and treatment of various pathological conditions, including neurodegenerative,[17] cardiovascular,[18] and autoimmune diseases,[19] as well as different types of cancer[20] (e.g. lymphoma, leukemia, and pancreatic, lung, and breast cancer). Technologies to detect specific nucleic acid sequences and the genetic variations within a human genome are often based on hybridization bioassays involving the use of DNA microarrays, in which thousands of probes are immobilized on a 2D surface. Optical,[21] electrochemical,[22] or gravimetric[23] detection is commonly used to monitor hybridization. Although widely used currently, they are limited to the specialized automated laboratory and their future commercial success is threatened by rapid next-generation sequencing.[24−27] The high cost of automation of complex multistep procedures, their inadequate detection limits, which often require target amplification by PCR, together with poor sensitivity and, particularly, the lack of reproducibility between devices[28−30] render such approaches unsuitable to the growing need for diagnostic tests at the point of care. Furthermore, such reproducibility is required in a simple test format suitable for direct interaction with live biological materials sampled from patients at the point of care.

Here, we demonstrate that *oligonucleotide−peptide* hydrogels can overcome such limitations. Unlike other polymers, many peptide hydrogelators form noncovalent 3D assemblies that spontaneously and reversibly produce hydrogels under physiological conditions, with excellent compatibility with live biological materials.[31−33] Peptide hydrogels also coassemble with modified components and display attached groups as probes on the surface of the peptide fibers that entangle to form the hydrogel. Functional groups are evenly spaced throughout the fibrous structure due to the stochastic nature of

Received: April 15, 2019
Accepted: June 27, 2019
Published: June 27, 2019

© 2019 American Chemical Society

DOI: 10.1021/acs.analchem.9b01841
Anal. Chem. 2019, 91, 10016−10025

self-assembly.[34] We find here that the ability to increase spatial separation between probes on the fiber surface minimizes unwanted *probe*−*probe* interactions, which may cause the poor sensitivity or false positives suffered by 2D microarray and biosensor devices. Functional hydrogel materials also have greater storage capacity than 2D systems,[35,36] which here improves the detection limits and sensitivity. Their self-assembling and self-healing nature[37,38] allowed our hydrogel detector to be dried and regenerated upon the addition of water, thereby providing simplicity of use, after long-term storage, protected against nuclease degradation.[35]

MATERIALS AND METHODS

Peptide Synthesis. Lys-Lys-Phe-Glu-Trp-Glu-Phe-Glu-Lys-Lys (**p2**$^{(+)}$), Mal-Gly-Gly-Lys-Lys-Phe-Glu-Trp-Glu-Phe-Glu-Lys-Lys (Mal-Gly-Gly-**p2**$^{(+)}$), and Val-Lys-Val-Lys-Val-Glu-Val-Lys (**v**$^{(+2)}$) were synthesized on a preloaded Fmoc-Lys-Boc-wang resin (300 mg, 0.1 mmol) using SPPS Fmoc chemistry. *N*,*N*-Diisopropylethylamine (DIPEA, 0.6 mmol, 6 equiv) and *N*,*N*,*N*′,*N*′-tetramethyl-*O*-(1*H*-benzotriazol-1-yl)-uronium hexafluorophosphate (HBTU, 0.3 mmol, 3 equiv) were used as activating and coupling agents, respectively. For maleimide-modified peptide (Mal-Gly-Gly-**p2**$^{(+)}$), *N*-maleoyl *β*-alanine modification was added at the N-terminus. Peptides were cleaved from the resin using TFA solution (TFA/TIPS/H_2O, 95/2.5/2.5; v/v/v 15 mL), precipitated in cold diethyl ether for 5 min. The peptides were separated by centrifugation and freeze-dried for 2 h. Peptides were then purified by reversed-phase HPLC (ACE 10 Preparative C-8 250 × 21.2 mm, PerkinElmer Nelson 1022, MA US) using 0.1% TFA in distilled water (eluent A) and 0.1% TFA in acetonitrile (eluent B) with a gradient increasing linearly from 10 to 100% of eluent B in 55 min at a flow rate of 1.5 mL/min (see Figure S1). Peptides were then characterized by ^{1}H NMR spectroscopy (Bruker Avance II+ NMR spectrometer, operating at proton frequencies of 400 MHz). In all cases, spectra were acquired using a BBI ^{1}H/D-BB Z-GRD Z8202/0347 probe and processed using Bruker software Topspin v2.0 or v2.1). Mass spectra of peptides and *peptide*−*oligonucleotide* conjugate were collected on a Waters SQ detector, mass spectrometer, electrospray/APCI ion source attached to an HPLC system (MA, USA), and matrix-assisted laser desorption/ionization-time of flight (MALDI-ToF/ToF) spectra were collected on a Bruker Daltonics Ultraflex II mass spectrometer (MA, USA), respectively. The peptides Mal-Acp-Gly-Gly-Val-Lys-Val-Lys-Val-Glu-Val-Lys (Mal-Acp-Gly-Gly-**v**$^{(+2)}$, Acp; aminocaproic acid linker) and Glu-Glu-Phe-Lys-Trp-Lys-Phe-Lys-Glu-Glu (**p1**$^{(-)}$) were purchased from Biomatik (Cambridge, Ontario, Canada), and excess trifluoroacetic acid (TFA) was removed via lyophilization from 10% (w/v) aqueous acetic acid.

Oligonucleotides. The following oligodeoxynucleotides were used in this study: $^{5'}$GGATTAGACTATCTCTGTGTTTGGCGAATGAAGTATCTTG$^{3'}$ (long perfect match), $^{5'}$TCTGTGTTTGGCGA$^{3'}$ (perfect match), $^{5'}$GGATTAGACTCTCTCTG**A**GTTTGGCGAATGAAGTATCTTG$^{3'}$ (mutant 1), $^{5'}$GGATTAGACTCTCTCTG**A**GT**A**TGGCGAATGAAGTATCTTG$^{3'}$ (mutant 2), $^{5'}$GGATTAGACTCTCTCTG**A**GT**A**TGGC**A**AATGAAGTATCTTG$^{3'}$ (mutant 3), $^{5'}$TTGTGTCTTAGC$^{3'}$ (scrambled sequence, *i.e.* complete mismatch), $^{5'}$F-T*CGATTCGCCAAACACAGAATCGA$^{3'}$-D (MB (terminal FAM), T* represents thiol modification) and $^{5'}$(CH$_2$)$_6$SS-F-T*CGATTCGCCAAACACAGAATCGA-D$^{3'}$(MB (internal FAM), T* represents (CH$_2$)$_6$SS modification). Oligodeoxynucleotides (see Table S1 and Figure S2 for sequences and representative structures, respectively) were purchased from ATDBio Ltd. (Southampton, U.K.). Prior to hybridization, oligonucleotides were desalted by gel filtration using GE Healthcare NAP-25 columns (Fisher Scientific UK Ltd., Loughborough, U.K.) using the protocol described in the manual.

Hydrogel Characterization. For negative staining transmission electron microscopy (TEM), hydrogel samples were formed from 20 mM (27 mg mL^{-1}) **p1**$^{(-)}$ and **p2**$^{(+)}$ peptides with and without oligonucleotide−peptide conjugate at pH 7.2 and incubated at 20 °C for 24 h. Samples were then diluted 1000-fold in doubly distilled water and placed onto glow-discharge treated 400 mesh carbon coated grids (Agar Scientific, Stansted, U.K.) for 1 min, washed three times with doubly distilled water, and negatively stained with freshly prepared and filtered 2% (w/v) uranyl acetate (Agar Scientific, Stansted, U.K.) for 1 min, blotting at each stage using Whatman filter paper. Samples were viewed and recorded on a Tecnai Biotwin TEM instrument (FEI, Oregon, USA) under an accelerating voltage of 100 kV, and imaged with a GATAN Orius CCD (Gatan, Oxford, U.K.). Fiber width and morphology analysis were performed using ImageJ. Rheological measurements of hydrogels were performed on a stress-controlled rheometer (Discovery HR-2, TA Instruments, Hertz, U.K.) using a 20 mm parallel plate. Samples were prepared by mixing equimolar concentrations (20 mM) of peptides **p1**$^{(-)}$ and **p2**$^{(+)}$ and incubated at 20 °C for 24 h prior to measurement. Hydrogel samples (180 μL) were loaded onto the stage, with the gap between the upper plate and stage set at 500 μm. Amplitude sweeps were undertaken at an oscillation frequency of 1 Hz between 0.02 and 40% strain. G' and G'' moduli were estimated in frequency sweeps between 0.01 and 15 Hz, at 0.2% strain.

Conjugate Synthesis. The peptide−oligonucleotide conjugates were synthesized as described by the reaction route in Figure S3 using a thiol−maleimide coupling reaction. Thiol-modified oligonucleotides with disulfide protecting groups were purchased from ATDbio Ltd. to prevent unwanted interference during synthesis, as well as the spontaneous formation of disulfide bonds. Prior to conjugation of the Mal-Gly-Gly-**p2**$^{(+)}$ to the thiol-modified oligonucleotide $^{5'}$F-T*CGATTCGCCAAACACAGAATCGA-D$^{3'}$(where T* is internal fluorescein and terminal thiol-functionalized thymidine nucleotide), the disulfide protecting group was reduced using a 10-fold excess of tris(2-chloroethyl) phosphate (TCEP) in 100 mM phosphate-buffered saline at pH 3 for 4 h, at room temperature. The maleimide-modified peptide, Mal-Gly-Gly-**p2**$^{(+)}$ (1.6 mg, 1 μmol), was dissolved in a minimal volume of DMSO (30 μL) and added to the oligonucleotide (0.04 μmol) in 70 μL of phosphate-buffered saline with gentle agitation. Conjugation of the thiol to maleimide proceeded spontaneously in aqueous media, adjusted to pH 7.0 with 0.5 M NaOH. DMSO (30% v/v) was included to disrupt fiber formation and minimize self-assembly. Reaction with a 25-fold excess of Mal-Gly-Gly-**p2**$^{(+)}$ for 4 h at room temperature gave the desired product (in 71% yield by HPLC, Figure S3B). The reaction was upscaled by increasing the component concentrations stochiometrically.

Crude materials were purified by reversed-phase HPLC using a Phenomenex Luna C-18 column. Eluents used included (A) 0.05 M $LiClO_4$ in water and (B) 0.05 M

DOI: 10.1021/acs.analchem.9b01841
Anal. Chem. 2019, 91, 10016−10025

$LiClO_4$ in acetonitrile, typically in a gradient from 0% to 50% of eluent B over 60 min. Oligonucleotide fractions were identified by detection of the UV absorbance at 260 nm and through their retention times (Figure S4). The collected fractions containing peptide−oligonucleotide conjugates were lyophilized. The lyophilizate was dissolved in D_2O and relyophilized prior to ^1H NMR characterization (Bruker Avance II+, 400 MHz). In all cases, oligonucleotide concentrations were measured using the UV absorbance at 260 nm (Varian Cary 4000 dual beam UV−vis spectrophotometer, Australia) using millimolar extinction coefficients as shown in Table S1. The conjugates were also characterized by mass spectrometry (MALDI-ToF/ToF) using a Bruker Daltonics Ultraflex-II instrument (MA, USA).

Sample Preparation. All samples for hybridization assays were prepared in aqueous 100 mM Tris buffer (pH 7.2) containing 200 mM KCl. Final peptide concentrations of 20 mM were used for hydrogel samples, unless stated otherwise. These were prepared by dissolving the peptide in half the total volume of water, followed by addition of the above hybridization buffer. After addition of the peptide−oligonucleotide conjugate, the pH was immediately adjusted to 7.2 with 5 M NaOH. The consequent reduction of buffer concentration in hydrogels by half (50 mM Tris pH 7.2, 100 mM KCl) did not affect hybridization and the resulting fluorescent signal, in comparison to solution studies.

Hybridization Studies. Following overnight incubation at 20 °C, oligonucleotide hybridization was assessed by increase in fluorescence at 519 nm (λ_{ex} 494 nm) at 20 °C (or 37 °C where stated) either in (a) 1 cm path-length quartz cuvettes, using a Shimadzu RF-5301 spectrofluorophotometer, operated with RF-5310PC software (Shimadzu Corporation, Kyoto, Japan) and equipped with temperature-controlled cell holder and 150 W xenon lamp, or (b) in microwell plates, using a Tecan Safire plate reader operated under Magellan Data Analysis Software (V.7).

Limit of Detection. The limit of detection (LoD) was estimated using a Tecan Safire plate reader in accordance with an established protocol.[39] Hybridization was detected over a 10 pM to 200 nM concentration range for the peptide−oligonucleotide conjugates and targets. Hydrogel molecular detectors with MB-Mal-Gly-Gly-$\mathbf{p2}^{(+)}$ conjugate doping levels ranging from 2.0×10^{-3} to 1.06×10^{-7} % were deposited in 250 μL aliquots into 96-well plates. Analyte samples (10 μL) containing the "perfect-match" (PM) DNA target were then introduced into the hydrogel molecular detector to achieve the same final molar concentration as the concentration of the recognition probe in each well. Following incubation for over 24 h at 20 °C, fluorescence measurements were taken. For comparison, similar studies were carried out in a solution containing 100 mM Tris and 200 mM KCl. Measurements were replicated as 20 freshly prepared samples with an equal amount of target analyte and molecular probe incorporated into the hydrogel and 20 blanks containing only the peptide hydrogel molecular detector with 10 μL buffer introduced on top. The mean value for "blank" samples ($Mean_{blank}$, $n = 20$) and standard deviations of the blank (SD_{blank}), as well as those of the low-concentration (10 pM) sample (SD_{lcs}, $n = 20$), were estimated from eqs 1 and 2, as presented in the Results and Discussion). Fluorescence was recorded at λ_{em} 523 nm following excitation at 494 nm.

Peptide Characterization. *$p2^{(+)}$, NH_2−Lys-Lys-Phe-Glu-Trp-Glu-Phe-Glu-Lys-Lys.* FT-MS: m/z 1395.720 $[M - 2H]^{-2}$; M_w = 1397.720 g mol^{-1} calculated for $[C_{68}H_{98}N_{15}O_{17}]$ (Figure S5B). ^1H NMR (Figure S6A) (400 MHz, D_2O, 25 °C, 0.1 μM TSP): δ 1.25−1.49 (m; 8H; 4 × Lys-CH_2^{γ}), 1.55−1.65 (m; 8H; 4 × Lys-CH_2^{δ}), 1.65−1.78 (apparent m; 8H; 4 × Lys-CH_2^{β}), 1.25−1.49 (m; 6H; 3 × Glu-CH_2^{β}), 1.49−1.78 (m; 8H; 4 × Lys-CH_2^{ε}), 1.78−2.06 (apparent m; 6H; 3 × Glu-CH_2^{γ}), 3.06−3.31 (apparent m; 2H; Trp-CH_2^{β}), 3.19−3.44 (m; 4H; 2 × Phe-CH_2^{β}), 4.21−4.43 (4H; 4 × Lys-CH^{α}), 4.21−4.44 (t; 3H; 3 × Glu-CH^{α}), 4.45−4.92 (t; 2H; 2 × Phe-CH^{α}), 4.45−4.92 (t; 1H; Trp-CH^{α}), 6.98−7.58 (apparent m; 5H; Trp-$CH^{\delta 1}$, $CH^{\epsilon 2}$, $CH^{\zeta 1}$, $CH^{\zeta 2}$, CH^{η}), 7.14−7.19 (apparent m; 4H; Phe-$CH^{\delta 1}$, $CH^{\delta 2}$), 7.14−7.19 (apparent m; 4H; Phe-$CH^{\epsilon 1}$, $CH^{\epsilon 2}$).

N-maleoyl-β-alanine-Gly-Gly-Lys-Lys-Phe-Glu-Trp-Glu-Phe-Glu-Lys-Lys. FT-MS: m/z 1659.785 $[M - 3H]^{-3}$; M_w = 1662.80 g mol^{-1} calculated for $[C_{79}H_{109}N_{18}O_{22}]$ (Figure S7). ^1H NMR (Figure S6B) (400 MHz, D_2O, 25 °C, 0.1 μM TSP): δ 1.25−1.49 (m; 8H; 4 × Lys-CH_2^{γ}), 1.55−1.65 (m; 8H; 4 × Lys-CH_2^{δ}), 1.65−1.78 (apparent m; 8H; 4 × Lys-CH_2^{β}), 1.25−1.49 (m; 6H; 3 × Glu-CH_2^{β}), 1.49−1.78 (m; 8H; 4 × Lys-CH_2^{ε}), 1.78−2.06 (apparent m; 6H; 3 × Glu-CH_2^{γ}), 3.06−3.31 (apparent m; 2H; Trp-CH_2^{β}), 3.19−3.44 (m; 4H; 2 × Phe-CH_2^{β}), 3.75 (t, 2H; maleimide N-CH_2), 4.21−4.43 (4H; 4 × Lys-CH^{α}), 4.21−4.44 (t; 3H; 3 × Glu-CH^{α}), 4.45−4.92 (t; 2H; 2 × Phe-CH^{α}), 4.45−4.92 (t; 1H; Trp-CH^{α}), 6.83 (s, maleimide CH_2═CH_2) 6.98−7.58 (apparent m; 5H; Trp-$CH^{\delta 1}$, $CH^{\epsilon 2}$, $CH^{\zeta 1}$, $CH^{\zeta 2}$, CH^{η}), 7.14−7.19 (apparent m; 4H; Phe-$CH^{\delta 1}$, $CH^{\delta 2}$), 7.14−7.19 (apparent m; 4H; Phe-$CH^{\epsilon 1}$, $CH^{\epsilon 2}$). Peptide charges were calculated at different pH values ranging from 1 to 14 using the expression derived from the Henderson-Hasselbalch equation as described elsewhere.[40]

Conjugate Characterization: Thiol-Modified MB ($^{5'}(CH_2)_6$-SS-F-TCGATTCGCCAAACACAGAATCGA-$D^{3'}$). MALDI-MS; m/z 8672.9; M_w = 8672.2 g mol^{-1} calculated for $[C_{300}H_{378}N_{100}O_{153}P_{25}S_2]$ (Figure S8A). ^1H NMR (Figure S9A) (D_2O with TSP (0.1 μM), 400 MHz): δ 0.79−2.78 (m, 97H; 24H; 24 × H2′ 24H; 24 × H2′′ sugar ring protons 12H; T(4 × CH_3) 14H; linker (7 × CH_2) 8H; fluorescein (4 × CH_2) 6H; Dabcyl (2 × CH_3) 6H; Dabcyl (1 × CH_2) 1H; Dabcyl (1 × CH) 2H; linker CH_2), 3.17−4.62 (m, 74H; 24H; 12 × H4, '24H;12 × H5′, 24H;12 × H5′′ 2H; linker), 4.94−6.87 (m, 32H; 24H, 24 × H1′ sugar ring protons, 7H,C (7 × H5), 1H; linker), 6.95−8.23 (m, 50H; 4H; G(4 × H8) 18H; A(9 × H2 + 9 × H8) 7H; C(7 × H6) 4H; T(4 × H6) 9H; fluorescein 8H; Dabcyl). Chemical shifts for 3H′ sugar ring protons are not included due to spectral distortion caused by presaturation of the HOD NMR signal.

MB-Peptide Conjugate: MB-Gly-Gly-Lys-Lys-Phe-Glu-Trp-Glu-Phe-Glu-Lys-Lys. MALDI-ToF: m/z 10060.2 [Li] adduct; M_w = 10054.8 g mol^{-1} calculated for $[C_{367}H_{463}N_{118}O_{172}P_{24}S^-]$ (Figure S10). ^1H NMR (Figure S9B): (D_2O with TSP (0.1 μM), 400 MHz): δ 0.79−2.78 (m, 151H; 8H; 4 × Lys-CH_2^{δ}, 8H; 4 × Lys-CH_2^{β}, 8H; 4 × Lys-CH_2^{ε}, 8H; 4 × Lys-CH_2^{γ}, 6H; 3 × Glu-CH_2^{γ}, 6H; 3 × Glu-CH_2^{β}, 4H; 2 × Phe-CH_2^{β}, 2H; Trp-CH_2^{β}, 4H; linker 2 × CH_2,8H; 4 × Lys-$CH2_{\delta}$, 8H; 4 × Lys-CH_2^{β}, 8H; 4 × Lys-CH_2^{γ}, 8H; 4 × Lys-CH_2^{ε}, 6H; 3 × Glu-CH_2^{β}), 3.17−4.62 (m, 24H;12 × H4′, 24H;12 × H5′, 24H;12 × H5′′, 2H; linker, 4H; 4 × Lys-CH^{α}, 3H; 3 × Glu-CH^{α}, 4H; 2 × Gly-CH_2^{α}, 1H; Trp-CH^{α}, 2H; 2 × Phe-CH^{α}, 2H; maleimide N-CH_2), 4.94−6.87 (m, 32H; 24H, 24 × H1′ sugar ring protons, 7H,C(7 × H5), 1H; linker), 6.95−8.23 (m, 65H; 4H; G(4 × H8) 18H; A(9 × H2 + 9 × H8) 7H; C(7 × H6) 4H; T(4 × H6) 9H; fluorescein

DOI: 10.1021/acs.analchem.9b01841
Anal. Chem. 2019, 91, 10016−10025

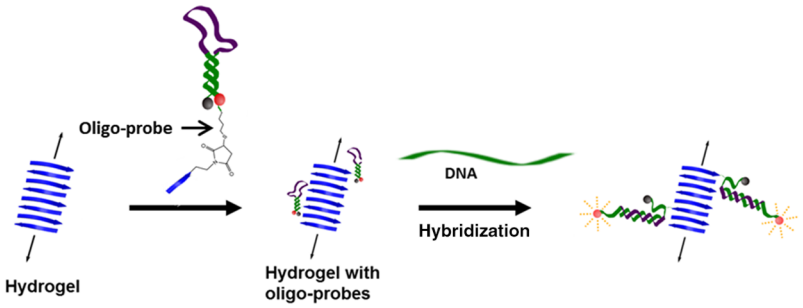

Figure 1. Design of a hydrogel incorporating oligonucleotide molecular probes bearing a recognition element and a sensing detector for sequence-specific detection of nucleic acids. Left: the nondecorated peptide hydrogel. middle: the nonhybridized peptide−oligonucleotide probes labeled with the fluorophore (**F**, in red) and quencher (**Q**, in black) are integrated into a hydrogel biomaterial in the form of folded structures (molecular beacons), which remain fluorescently silent due to effective quenching of **F** by closely located **Q**. Right: the decorated hydrogel incorporating *peptide−oligonucleotide* molecular probes allows capture of the biotarget (DNA or RNA) by Watson−Crick hydrogen bonding between regions complementary to the oligonucleotide recognition motifs, which triggers probe unfolding and separation of the **F** and **Q** to allow **F** to fluoresce.

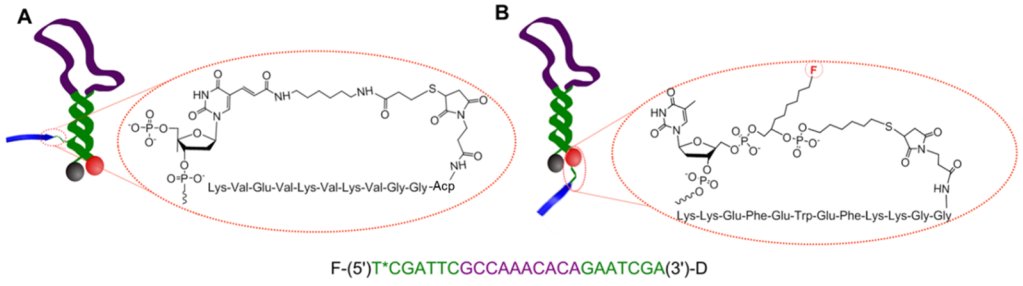

Figure 2. Attachment of peptide component and fluorophore to the MB probe. (A) The peptide−MB conjugate was synthesized by linking the internal thiol-dT nucleotide to the maleimide functional group attached at the N-terminus of the amphiphatic $\mathbf{v}^{(+2)}$ peptide (Mal-Acp-Gly-Gly-$\mathbf{v}^{(+2)}$). In this case, fluorophore (**F**) was attached at the 5′-terminus of the oligonucleotide. (B) The peptidyl−MB conjugate was synthesized from the oligonucleotide labeled with an internal fluorophore (**F**) and bearing the 5′-terminal thiol group, which was conjugated to the ionic peptide (Mal-Gly-Gly-$\mathbf{p2}^{(+)}$) via an *N*-maleoyl-*β*-alanine functional group. In both cases, the quencher (dabcyl) was attached at the 3′-terminus of MB. The oligonucleotide is color-coded to show the loop (purple) and stem region (green) of the MB. The peptide is shown in blue. Fluorescein and dabcyl are denoted as **F** and **D** and shown as red and black spheres, respectively. The peptide was attached using thiol-−aleimide chemistry between a thiol-functionalized nucleotide, denoted with an asterisk, and a maleimide-functionalized self-assembling peptide.

8H; Dabcyl 5H; Trp-$CH^{\delta1}$, $CH^{\epsilon2}$, $CH^{\zeta1}$, $CH^{\zeta2}$, CH^{η} 4H; Phe-$CH^{\delta1}$, $CH^{\delta2}$ 4H; Phe-$CH^{\epsilon1}$, $CH^{\epsilon2}$ 1H; Phe-CH^{ζ}).

RESULTS AND DISCUSSION

Our hydrogel molecular detector required precise integration of biorecognition into the controlled self-assembly of the peptide fibers of the hydrogel, in order to achieve direct detection of unmodified, biologically relevant nucleic acid sequences, without any amplification. To achieve this, we used here a molecular beacon (MB) concept (Figure 1), employing here fluorescein (as fluorophore, **F**) and dabcyl (as quencher, **D**). Binding of a complementary unlabeled target generated a fluorescent signal, due to the spatial separation of the *fluorescein−dabcyl* FRET pair, triggered by hybridization to the loop and/or the fragment of the stem region of the MB recognition element. The FRET pair was covalently attached to respective terminal groups of the recognition oligonucleotide (with **F** and **D** located at the 5′-end and 3′-end, respectively). A third attachment point was used to conjugate the MB recognition element to the peptide modification decorating the peptide hydrogel fibers.

Peptide hydrogels formed by the amphipathic peptide Val-Lys-Val-Lys-Val-Glu-Val-Lys ($\mathbf{v}^{(+2)}$- peptide) did not provide suitable fluorescence signals upon hybridization with the target sequence. The MB-peptide conjugate MB-Mal-Acp-Gly-Gly-$\mathbf{v}^{(+2)}$ formed a seven-residue staple region (i.e., F-$^{5'}$T*CGA-TTCGCCAAACACAGAATCGA$^{3'}$-D, where the nucleotides that formed the stem region are underlined). The detailed chemical structure of such a MB-Mal-Acp-Gly-Gly-$\mathbf{v}^{(+2)}$ conjugate is shown in Figure S2A. The base denoted with an asterisk was a thymidine with a modified aromatic base that allowed attachment of a thiol group via a flexible linker at position 5 (see Figure 2A and Figure S2A). Synthesis of the peptide−oligonucleotide conjugate MB-Mal-Acp-Gly-Gly-$\mathbf{v}^{(+2)}$ was achieved using thiol−maleimide chemistry between the thiol-modified MB and N-terminally modified $\mathbf{v}^{(+2)}$-peptide (see Figure S3A for chemistry). The successful syntheses of the Mal-Acp-Gly-Gly-$\mathbf{v}^{(+2)}$ peptide and MB-Mal-Acp-Gly-Gly-$\mathbf{v}^{(+2)}$ conjugate were confirmed using reversed-phase HPLC, mass spectrometry (see Figure S11B), and ^{1}H NMR spectroscopy (see Figures S12B and S13B and Materials and Methods for details).

Hydrogels formed by $\mathbf{v}^{(+2)}$-peptide in both the absence and presence of the MB-Mal-Acp-Gly-Gly-$\mathbf{v}^{(+2)}$ conjugate (0.006% doping level) were characterized using transmission electron microscopy (TEM, Figure S14). Inefficient quenching of the fluorophore by the quencher in the unhybridized state of the MB-Mal-Acp-Gly-Gly-$\mathbf{v}^{(+2)}$ conjugate appeared to give a higher background signal of the unbound probe and poor overall fluorescence response upon its hybridization with the target sequence (typically only 10-fold fluorescence increase above the background, data not shown). Moreover, the uncontrolled

DOI: 10.1021/acs.analchem.9b01841
Anal. Chem. 2019, 91, 10016−10025

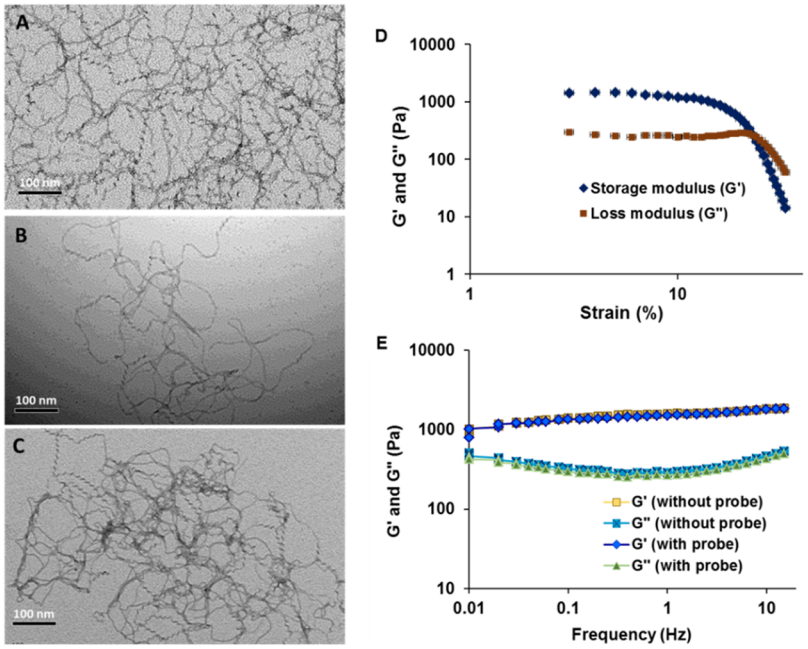

Figure 3. Characterization of peptide hydrogel using TEM and an oscillatory shear rheometer. (A) TEM images showing nanofibers formed by $\mathbf{p1}^{(-)}$ (Glu-Glu-Phe-Lys-Trp-Lys-Phe-Lys-Glu-Glu) and $\mathbf{p2}^{(+)}$ (Lys-Lys-Phe-Glu-Trp-Glu-Phe-Glu-Lys-Lys) peptides (1:1 mol ratio; 20 mM, 100-fold diluted) used to fabricate the hydrogel molecular detector in the absence (B) and presence (C) of the DNA recognition motif. (A) Hydrogel network resulting from the self-assembly of ionic-complementary peptides into nanofibers with twisted helical structures along the fiber axes. Samples shown in (B) and (C) were diluted 1000-fold to visualize the less dense fiber meshwork. (B) Peptide hydrogel formed from unmodified ionic-complementary peptides $\mathbf{p1}^{(-)}$ and $\mathbf{p2}^{(+)}$ at pH 7 (average dimeter 4.7 nm, SD = 1.2, n = 224). (C) Peptide fibers resulting from probe-functionalized hydrogel. No significant effect in fiber morphology was observed by incorporation of MB−peptide conjugate into the hydrogel (average dimeter 4.5 nm, SD = 1.1, n = 326). The hydrogel sample was prepared from 10 mg mL^{-1} of peptides at pH 7.2. Hydrogel carries a neutral charge under molecular sensing working conditions. (D) Amplitude sweep of a standard hydrogel sample prepared from 20 mM concentrations of peptides ($\mathbf{p1}^{(-)}$+ $\mathbf{p2}^{(+)}$). Storage (G') and loss (G'') moduli showed their independence at 1% strain. (E) Frequency sweeps of peptide hydrogel samples with and without the addition of the highest concentration (0.5 μM, 0.01% relative to base peptides) of the recognition probe used in this study, at 1% strain from 0.01 to 15 Hz. Average data of three independent experiments are presented.

gelation of the amphipathic peptide $\mathbf{v}^{(+2)}$ during its conjugation to the MB and the extremely low reaction yield (only 7%) in the synthesis of the MB-Mal-Acp-Gly-Gly-$\mathbf{v}^{(+2)}$ conjugate made this design unsuitable for practical use. This was resolved by precise control of the gelation of the peptide component using the complementary ionic peptides[41] $\mathbf{p1}^{(-)}$ (Glu-Glu-Phe-Lys-Trp-Lys-Phe-Lys-Glu-Glu) and $\mathbf{p2}^{(+)}$ (Lys-Lys-Phe-Glu-Trp-Glu-Phe-Glu-Lys-Lys). These ionic peptides provided an alternating pattern of hydrophobic (e.g. Phe and Trp) and hydrophilic (e.g., Lys and Glu) amino acids, such that the peptides were flanked with oppositely charged residues. Here, $\mathbf{p1}^{(-)}$ presented the negatively charged [Glu-Glu] blocks at both the N- and C-termini, whereas the $\mathbf{p2}^{(+)}$ peptide was flanked with positively charged [Lys-Lys] blocks from both ends of the sequence. The absence of homotypic interactions prompt the "sticky faces" of $\mathbf{p1}^{(-)}$ and $\mathbf{p2}^{(+)}$ to self-assemble into antiparallel β-sheets capable of forming fibrils.[41] Peptide $\mathbf{p1}^{(-)}$ carried a net negative charge of −1 due to the predominance of Glu residues over Lys residues, whereas $\mathbf{p2}^{(+)}$ was positively charged +1, as more Lys residues than Glu residues were in its structure.

The MB-Mal-Acp-Gly-Gly-$\mathbf{v}^{(+2)}$ conjugate incorporated the thiol group internally into the recognition oligonucleotide ("internal-thiol"), which led to a low (7%) conjugate yield (see Figures S3A and S4 in the Supporting Information), as this functional group was presumably buried within the structure and less accessible for reaction with the peptide. When, however, we swapped the attachment point of the peptide with that of the fluorophore, in such a way that the thiol linker ($-(CH_2)_6$-SH) became located at the 5′-terminal position of the MB probe ("terminal-thiol", see Figure 2B for the design and Figure S2B for structural details), we considerably (>10-fold) improved the final reaction yield (71%). In addition, the closer location of the fluorophore and quencher in this design allowed a reduced background noise for the unhybridized MB, thereby contributing to the improved sensitivity and LoD reported below.

Favorable conditions for efficient conjugation with MB were provided by selection of the $\mathbf{p2}^{(+)}$ peptide for conjugation, because it has a relatively high critical gelation concentration in comparison to that of $\mathbf{p1}^{(-)}$ (i.e., 35 and 65 mM for $\mathbf{p1}^{(-)}$ and $\mathbf{p2}^{(+)}$, respectively; see Table S2 in the Supporting Information). The peptide was functionalized with a maleimide moiety to produce Mal-Gly-Gly-$\mathbf{p2}^{(+)}$ for conjugation with the MB probe. A two-glycine spacer was added to the peptide sequence to provide a flexible linker between the peptide fibers and the DNA recognition motif, in order to avoid agglomeration of biomolecules at the N-terminus following conjugate synthesis. Mal-Gly-Gly-$\mathbf{p2}^{(+)}$ was synthesized using standard Fmoc-based solid-phase synthesis and functionalized with N-maleoyl-β-alanine at the N-terminus, as we described previously.[35] Synthesis of the *peptide−oligonucleotide* conjugate MB-Mal-Gly-Gly-$\mathbf{p2}^{(+)}$ was performed using a thiol−maleimide chemistry (see Materials and Methods) between the thiol-modified MB and N-terminally labeled peptide Mal-Gly-Gly-$\mathbf{p2}^{(+)}$ (see Figure 2 and Figure S3B for

DOI: 10.1021/acs.analchem.9b01841
Anal. Chem. 2019, 91, 10016−10025

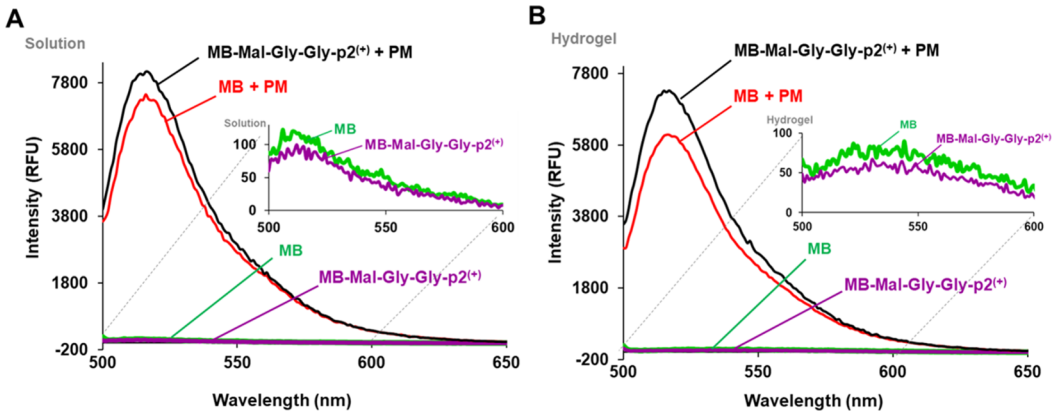

Figure 4. Fluorescence detection of hybridization of analyte sequence in (A) solution and (B) hydrogel. (A) The peptide−oligonucleotide conjugate MB−Mal-Gly-Gly-$\mathbf{p2}^{(+)}$ (magenta) and MB (green) were fluorescently silent in isolation (i.e. prior to addition of the analyte sequence). The addition of the "perfect-match" target (PM) led to hybridization with the recognition motif of the probe, which triggered fluorescence from MB−Mal-Gly-Gly-$\mathbf{p2}^{(+)}$ (black) or MB (red). All components were at 0.5 μM concentration. Hydrogel was prepared at pH 7.2 using 20 mM of base peptides ($\mathbf{p1}^{(-)}$+$\mathbf{p2}^{(+)}$). Fluorescence was recorded at λ_{em} 519 nm following excitation at λ_{ex} 494 nm. Inserts present the magnified parts of the spectra to show the background signal from free MB and conjugate MB−Mal-Gly-Gly-$\mathbf{p2}^{(+)}$.

the design and synthetic route, respectively). Successful conjugation of the Mal-Gly-Gly-$\mathbf{p2}^{(+)}$ to the oligonucleotide was confirmed (i) by the change in the HPLC retention time from 22.9 min (thiol−oligonucleotide) to 24.5 min (conjugate) (see Figure S4), (ii) by mass spectrometry of the purified product (see Table S1 and Figure S10), (iii) by the disappearance of the ^{1}H NMR signal at 6.78 ppm, which was previously observed for the maleimide CH═CH protons, and (iv) by comparison of the ^{1}H NMR recorded for the reaction product with those of the starting materials (Figures S9A,B).

Hydrogel Characterization. The hydrogel was prepared by mixing equimolar concentrations (20 mM) of unfunctionalized $\mathbf{p1}^{(-)}$ and $\mathbf{p2}^{(+)}$ at pH 5, followed by adjustment to pH 7.2, which triggered formation of a solid self-supporting hydrogel within 1 min at room temperature. TEM of the peptidyl−-oligonucleotide hydrogel showed that the peptide fiber morphology was not affected by the incorporation of the peptide−oligonucleotide conjugate, MB-Mal-Gly-Gly-$\mathbf{p2}^{(+)}$ (see Figure 3), at the highest doping level used here (0.0025% relative to the base peptides). Peptide fibers in the naked and decorated hydrogels had average diameters of 4.7 and 4.5 nm, respectively (4.7 nm, SD = 1.2, SE = 0.08, n = 224; 4.5 nm, SD = 1.1, SE = 0.065, n = 326, see Figure 3B,C). Microscopic analysis revealed twisted helical structures and defined spiraling of peptide fibers along the axes. This twisting pattern of fibers can be attributed to the chiral folding of peptide chains, persumbly caused by the strength of specific interactions between the complementary peptide components. For comparison, the amphipathic peptide $\mathbf{v}^{(+2)}$, with and without the addition of peptide−oligonucleotide conjugate, MB-Mal-Acp-Gly-Gly-$\mathbf{v}^{(+2)}$ (0.006% relative to the base peptide), showed thicker fibers with slightly larger average diameters of 5.27 and 5.34 nm, respectively (SD = 0.54, n = 50; SD = 0.68, n = 50; Figure S14).

Mechanical characterization of the peptide hydrogel formed by $\mathbf{p1}^{(-)}$ (Glu-Glu-Phe-Lys-Trp-Lys-Phe-Lys-Glu-Glu) and $\mathbf{p2}^{(+)}$ (Lys-Lys-Phe-Glu-Trp-Glu-Phe-Glu-Lys-Lys) peptides was carried out by oscillatory shear rheometry, in both amplitude and frequency-sweep modes to determine the storage (G') and loss moduli (G''). The linear viscoelastic region (LVR), quantized for hydrogel in amplitude-sweep mode, showed the moduli independence at 1% strain (see Figure 3D), which was chosen for frequency-sweep studies. No significant difference in hydrogel mechanical strength was observed with and without the addition of the highest concentration of the recognition probe used in this study (0.0025% relative to the base peptides), suggesting that incorporation of the recognition element did not interfere with the bulk physical properties of the peptide hydrogel (Figure 3E), although the possibility of some local changes in the peptide fiber architecture cannot be excluded.

Hybridization Studies. The "perfect-match" (PM) target for the designed probe was optimized by ensuring that its sequence ($^{5'}$TCTGTGTTTGGCGA$^{3'}$) is complementary primarily to the loop region of the MB probe. Prior to hybridization with the "perfect-match" analyte sequence $^{5'}$TCTGTGTTTGGCGA$^{3'}$, unconjugated MB and MB−Mal-Gly-Gly-$\mathbf{p2}^{(+)}$ conjugate were almost completely fluorescently silent in isolation (Figure 4). The hydrogel environment provided more effective quenching of the fluorophore by the quencher in comparison to that seen in solution (1.9-fold lower for MB and 2.7-fold for MB−peptide conjugate, Figure 4A,B). Upon exposure to perfect match DNA ($^{5'}$TCTGTGTTTGGCGA$^{3'}$), this low fluorescence background allowed the large, more than 2 orders of magnitude increase in fluorescence (106-fold for incorporated MB and 166-fold for immobilized MB-Mal-Gly-Gly-$\mathbf{p2}^{(+)}$, Figure 4A,B). The hydrogel environment amplified the fluoresence signal by considerably improving the signal to noise (S/N) ratio. In addition to the reduced background, the fluorescence intensity of the reporter group may also be improved within the hydrogel environment, by aligning the quencher (**Q**) and fluorophore (**F**) at a comparably greater distance after hybridization events. The positively charged surfaces of hydrogel fibers may also attract the negatively charged analyte DNA and increase their "effective" concentrations around the recognition probe, thereby leading to more efficient hybridization.

"Fishing"* for Sequence Fragments.** The hydrogel molecular detector could *"fish out"* and detect a "perfect-match" target (14 nt) when it was embedded in the central part of a longer (40 nt) oligonucleotide sequence $^{5'}$GGATTAGACTATCTCTGTGTTTGGCGA***ATGAAGTATCTTG$^{3'}$, where the "perfect-match" target sequence is shown in bold italics (Figure 5). In the hydrogel environment at 20 °C

DOI: 10.1021/acs.analchem.9b01841
Anal. Chem. 2019, 91, 10016−10025

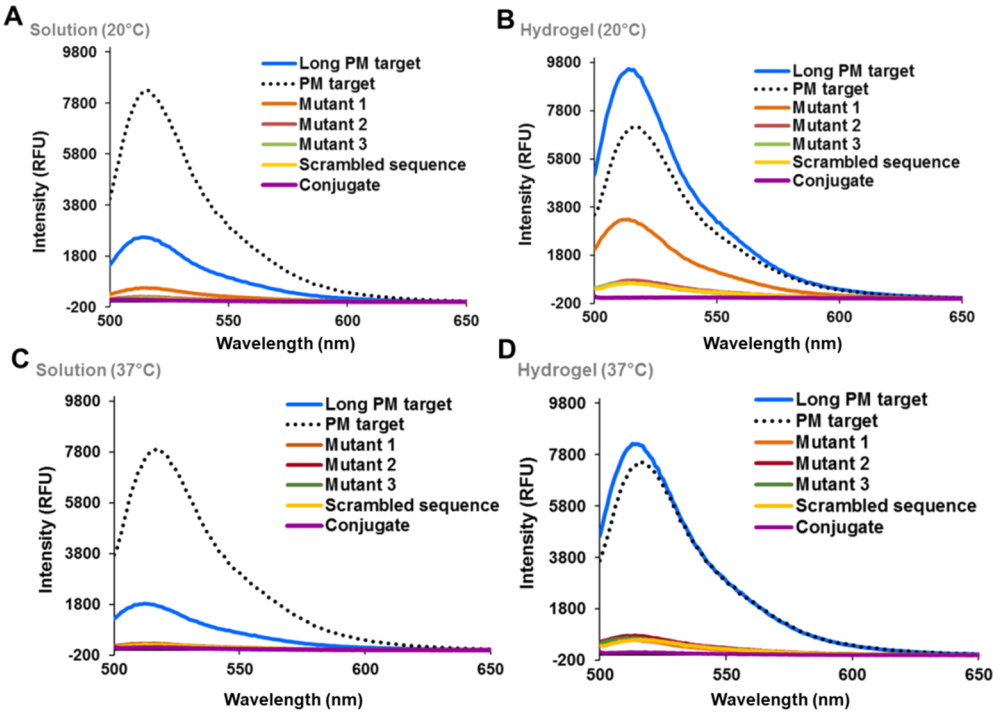

Figure 5. Comparison of fluorescence detection of hybridization between the recognition motif with the long "perfect-match" sequence and with the mismatches in solution (A and C) and in peptide-hydrogel (B and D) at 20 °C (A and B) and at 37 °C (C and D) for peptides ($\mathbf{p1}^{(-)}$ + $\mathbf{p2}^{(+)}$) at pH 7.2. For comparison, the response triggered by the addition of the short "perfect-match" from Figure 4 is shown (black dotted lines). The peptide−oligonucleotide conjugate MB−Mal-Gly-Gly-$\mathbf{p2}^{(+)}$ alone (magenta) was fluorescently silent prior to addition of the analyte sequence. The level of fluorescence response strongly depended on the nature of the analyte sequences: the long "perfect-match" (Long PM target, blue), mutant 1 (orange), mutant 2 (deep red), mutant 3 (green), and scrambled sequence (yellow). Fluoresence was recorded at λ_{em} 519 nm following excitation at λ_{ex} 494 nm.

(Figure 5B), the addition of this long "perfect-match" sequence led to a large enhancement of the fluorescence signal (265-fold), which was even more pronounced than that seen after introducing the short (14 nt) fully matched target. Interestingly, the hybridization of the long "perfect-match" sequence in solution showed a comparatively modest (25-fold) fluorescence increase under similar conditions (cf. Figure 5A vs Figure 5C). Multiple, weak structural interactions within the long DNA sequences (e.g. due to imperfect *intra-* and/or *inter*molecular Watson−Crick hydrogen bonding) can be stabilized in aqueous solution, thus representing significant barriers for hybridization with the MB recognition motifs. The hydrogel environment seemed to minimize the probability of forming such structural elements, which led to a better accessibility of the target regions for recognition by the MB and precise hybridization. In addition, the conformational constraints induced in the duplex formed with a longer target following the hybridization events are likely to be more pronounced in the hydrogel environment than those in the free solution, which would lead to better spatial separation of the reporter groups (**F** and **Q**) from each other, thereby contributing to a significant enhancement of the fluorescent signal.

Ability To Discriminate Mismatches. Finally, we evaluated whether the designed peptide−hydrogel molecular detector can be used to discriminate "perfect-match" sequences, particularly single-nucleotide mutations, as SNPs are linked to various monogenic and complex diseases.[13−16] The long "perfect-match" analyte sequence $^{5'}$GGATT-AGACTATC***TCTGTGTTTGGCGA***ATGAAGTATCTTG$^{3'}$ was "mutated" at one, two, or three different positions to produce three "mutant" sequences. Mutant 1 ($^{5'}$GGATT-AGACTCTC***TCTGAGTTTGGCGA***ATGAAGTATCTTG$^{3'}$) had ***A*** (underlined) as a replacement for ***T*** at position 18. In the sequence of mutant 2 ($^{5'}$GGATTAGACTCTC***TC-TGAGTATGGCGA***ATGAAGTATCTTG$^{3'}$) two thymidine residues at positions 18 and 21 were replaced with adenosine residues, whereas mutant 3 ($^{5'}$GGATTAGACTCTC***TC-TGAGTATGGCAA***ATGAAGTATCTTG$^{3'}$) had an additional third mutation by replacement of ***G*** at position 26 with ***A*** (see Table S1 for a full list of sequences). A negative control was compared, using a scrambled sequence ($^{5'}$TTGTGT-CTTAGC$^{3'}$), which had no complementarity with the MB recognition motif. Each analyte sequence was added to a peptide−hydrogel molecular detector preloaded with MB-Mal-Gly-Gly-$\mathbf{p2}^{(+)}$ conjugate in separate incubates, as described earlier for the long "perfect-match" target. Similar studies were carried out in free solution to compare the performance with the hydrogel environment (see Materials and Methods for full details). Gratifyingly, very little difference was observed between the background fluorescence of the MB-Mal-Gly-Gly-$\mathbf{p2}^{(+)}$ conjugate and the fluorescent signal developed after addition of mutant 2, or mutant 3, or the "scrambled" sequence, both in solution and hydrogel (Figure 5A,B). Smaller increases in fluorescence were observed for mutant 1, both in solution (5-fold) and hydrogel (78-fold), at 20 °C, presumably indicating a weak hybridization of the mismatched target with the recognition probe (Figure 5A,B). However, an increase in temperature from 20 to 37 °C allowed us to minimize the probability of hybridization through "nonperfect"

DOI: 10.1021/acs.analchem.9b01841
Anal. Chem. 2019, 91, 10016−10025

interactions and to discriminate a single mismatch (e.g., mutant 1) from the "perfect-match" sequence. Indeed, at 37 °C the fluorescence response upon hybridization with mutant 1 was 10.6-fold and 14.5-fold lower in the solution and hydrogel, respectively, in comparison with the signal generated by the long "perfect-match" target under identical conditions (see Figure 5C,D). Under stringent conditions (e.g., temperature raised to 37 °C), the designed molecular detector could discriminate SNPs related to various pathological disorders.

To demonstrate the potential of our molecular sensor to *"fish out"* the perfect match sequence from complex analytical samples, we used an "oligo mix" system to mimic a multimacromolecular environment containing several RNA and DNA sequences alongside the isolated PM targets. Either PM target or long PM target was incorporated into the "oligo mix" sample consisting of various DNA/RNA components at equimolar concentrations (0.5 mM): miR-21 RNA target ($^{5'}$UAGCUUAUCAGACUGAUGUUGA$^{3'}$), miR-21 mismatch 1 ($^{5'}$UAGCU**A**AUCAGACUGAUGUUGA$^{3'}$), miR-21 mismatch 2 ($^{5'}$UAGCU**A**AUCAGACUG**G**UGUUGA$^{3'}$), miR-21 mismatch 3 ($^{5'}$U**U**GCUUAUCAGACUGAUGUUGA$^{3'}$), miR-21 mismatch 4 ($^{5'}$UAGCUUAUCAGACUGAUGUU**C**A$^{3'}$), and scrambled sequence ($^{5'}$TTGTGTCTTAGC$^{3'}$). Such an "oligo mix" containing either PM target or long PM target was then added to the test sample preloaded with the MB-Mal-Gly-Gly-**p2**$^{(+)}$ conjugate (Figure S15) either in solution (Figure S15A) or in hydrogel format (Figure S15B) and tested under conditions identical with those described earlier. The fluorescence signal generated from the "oligo mix" containing "perfect match" sequences (either PM target or long PM target) completely replicated the fluorescence response observed upon addition of the isolated short (14 nt) or longer (40 nt) "perfect match" targets (Figure S15). This demonstrated the ability of our molecular detector to recognize and detect the target squence in the presence of other macromolecular components.

Limit of Detection (LoD). The lowest limit at which peptide−hydrogel molecular detection could be reliably measured was determined through a series of hybridization experiments conducted with MB−Mal-Gly-Gly-**p2**$^{(+)}$ conjugate and analyte (1:1), over a concentration range of 200 nM to 10 pM, which corresponded to hydrogel doping levels of 2.0×10^{-3} to 1.06×10^{-7}%. The lowest concentration of target that was visually distinguishable from the background using the peptide−hydrogel molecular sensor was 10 pM (Figure S16). The limit of the blank (LoB) and limit of detection (LoD) for solution and hydrogel molecular detector were estimated (see Materials and Methods for details) by applying eqs 1 and 2:

$$\mathrm{LoB} = \mathrm{Mean}_{\mathrm{blank}} + 1.645(\mathrm{SD}_{\mathrm{blank}}) \quad (1)$$

$$\mathrm{LoD} = \mathrm{LoB} + 1.645(\mathrm{SD}_{\mathrm{lcs}}) \quad (2)$$

The calculated LoB was 4.7 pM, and the LoD of 6.8 pM was 21-fold lower than that estimated for the MB−Mal-Gly-Gly-**p2**$^{(+)}$ conjugate in solution (LoD = 142 pM). Moreover, the LoD of this biologically relevant hydrogel molecular detector was notably lower than that estimated for our earlier design (22 pM), which was built using the amphipathic base peptide **v**$^{(+2)}$.[35] The amphipathic peptide **v**$^{(+2)}$ formed the hydrogel with slightly thicker nanofibers in comparison to the ionic complementary peptides (**p1**$^{(-)}$ and **p2**$^{(+)}$). This may have resulted in the formation of a more constrained and dense fiber architecture by the amphipathic peptide **v**$^{(+2)}$, which may have led to the reduced mobility of macromolecules (e.g., DNA probes or DNA targets) on diffusion through the hydrogel channels, thus hindering the molecular interactions and performance of molecular detection in the amphipathic peptide hydrogel.

In contrast, the mutual orientation of the key structural components within the MB detector (i.e., fluorophore, quencher, and peptide) was the most important factor underpinning the success of the molecular detector in the ionic peptide hydrogel. Indeed, the refined mutual location of all the key players of the molecular detector (i.e., **F**, **Q**, and peptide) presumably improved fluorophore quenching within the unhybridized probes, thus leading to a decreased background signal and improved overall performance upon hybridization with the target. The higher detection signal (S/N 238:1) in comparison to that in solution (S/N 25:1) was largely attributable to a reduction in the background fluorescence signal, leading to the observed increase in the S/N ratio. Further, the ionic peptide hydrogel environment also seemed to optimize the alignment of the MB-Mal-Gly-Gly-**p2**$^{(+)}$ probe on hybridizing with the target sequence, in such a way as to minimize residual FRET between **F** and **Q**, thus leading to the enhancement of the fluorescence signal after binding with the target.

CONCLUSION

We have demonstrated here the key structural aspects important for peptide hydrogel molecular detection of targeted nucleic acids to be effective at low levels with high specificity. Our hybrid *oligonucleotide−peptide* hydrogel detector was able to *"fish out"* the perfect match target sequences even from complex analytical sample in the presence of other RNA and DNA sequences. It discriminated a "perfect-match" target from mismatched sequences down to a single nucleotide mutation, even when this mutation was embedded in a longer oligonucleotide sequence, thus demonstrating its potential to detect SNPs. Optimized assay stringency conditions provided a simple *"on/off"* signal for particular single-nucleotide mutations. The simplicity and robustness of this hydrogel detector appear well suited to evaluation next in live biological materials.

The modular nature of our hydrogel molecular detector design can be readily adapted to other molecular targets simply by changing the molecular recognition element of the MB−conjugate to the desired aptamer for the detection and quantification of pathogenic DNA or microRNA sequences. This molecular design is also suited to different combinations of *fluorophore−quencher* FRET couples or various excimer and exciplex partners to provide an opportunity for the simultaneous detection of multiple analyte sequences.

ASSOCIATED CONTENT

Supporting Information

The Supporting Information is available free of charge on the ACS Publications website at DOI: 10.1021/acs.analchem.9b01841.

Sequences of the oligonucleotides, peptides, and peptide−oligonucleotide conjugates, gelation concentration of peptides, HPLC chromatograms of peptides, chemical structures of peptide−oligonucleotide conjugates, reaction routes for conjugate synthesis, HPLC chromatograms of oligonucleotide materials, mass

DOI: 10.1021/acs.analchem.9b01841
Anal. Chem. 2019, 91, 10016−10025

spectra, NMR spectra, TEM of amphipathic peptide, *fishing out* perfect match sequences from complex oligonucleotide mixtures, LoD of the peptide hydrogel sensor, and peptide charge calculations (PDF)

AUTHOR INFORMATION

Corresponding Author

*E-mail for E.V.B.: Elena.V.Bichenkova@manchester.ac.uk.

ORCID

Alberto Saiani: 0000-0002-5504-8306

Elena V. Bichenkova: 0000-0002-4747-5543

Present Address

§Present address of P.J.S.K.: Malvern Panalytical Ltd., Enigma Business Park, Grovewood Road, Malvern, WR14 1XZ, UK.

Author Contributions

E.V.B., D.J.C., A.S. and A.F.M. conceived and designed the experiments. Peptide and conjugate materials were synthesized and characterized by NMR and mass spectrometry by S.Y. and P.J.S.K. and L.T.T. under the supervision of H.S.A. and E.V.B. UV and fluorescent studies were carried out by S.Y. and P.J.S.K. under the direction of E.V.B. and D.J.C. TEM analysis of hydrogel materials was carried out by S.Y. and P.J.S.K. under the direction of A.F.M. and A.S. S.Y. undertook mechanical characterization of hydrogels. E.V.B., D.J.C., S.Y., A.S. and A.F.M. analyzed the data and cowrote the paper.

Notes

The authors declare no competing financial interest.

ACKNOWLEDGMENTS

This work was supported by the Wellcome Trust (grant number: 105610/Z/14/Z, "Research Consortia" Scheme), BBSRC (grant number: BB/K012622/1), and Russian Science Foundation Grant (grant number: 14-44-00068). The doctoral training program of S.Y. was supported by a Chief Minister Merit Scholarship (CMMS), Pakistan. The authors thank the EPSRC National Mass Spectrometry Centre in Swansea for MS analysis of the peptidyl−oligonucleotide conjugate samples and ATDbio Ltd (in particular, Dr. Daniel Singleton) for providing mass spectra of the oligonucleotides. The authors are grateful to Neil O'Hara for his technical support while using optical and analytical instrumentation.

REFERENCES

(1) Chiang, A. P.; Beck, J. S.; Yen, H. J.; Tayeh, M. K.; Scheetz, T. E.; Swiderski, R. E.; Nishimura, D. Y.; Braun, T. A.; Kim, K. Y. A.; Huang, J.; Elbedour, K.; Carmi, R.; Slusarski, D. C.; Casavant, T. L.; Stone, E. M.; Sheffield, V. C. *Proc. Natl. Acad. Sci. U. S. A.* **2006**, *103*, 6287−6292.

(2) Giannini, C.; Dalla Man, C.; Groop, L.; Cobelli, C.; Zhao, H.; Shaw, M. M.; Duran, E.; Pierpont, B.; Bale, A. E.; Caprio, S.; Santoro, N. *Diabetes Care* **2014**, *37*, 475−482.

(3) Brown, A.; Hirsch, R.; Laor, T.; Hannon, M. J.; Levesque, M. C.; Starz, T.; Francis, K.; Kwoh, C. K. *Arthritis Care Res.* **2012**, *64*, 1846−1854.

(4) Steinberg, S.; Stefansson, H.; Jonsson, T.; Johannsdottir, H.; Ingason, A.; Helgason, H.; Sulem, P.; Magnusson, O. T.; Gudjonsson, S. A.; Unnsteinsdottir, U.; Djurovic, S.; Sando, S. B.; White, L. R.; Knudsen, G. P.; Westlye, L. T.; Selbæk, G.; Giegling, I.; Hampel, H.; Hiltunen, M.; Levey, A. I.; Andreassen, O. A.; Rujescu, D.; Jonsson, P. V.; Bjornsson, S.; Snaedal, J.; Stefansson, K. *Nat. Genet.* **2015**, *47*, 445−447.

(5) Hoban, M. D.; Cost, G. J.; Mendel, M. C.; Romero, Z.; Kaufman, M. L.; Joglekar, A. V.; Ho, M.; Lumaquin, D.; Gray, D.; Lill, G. R.; Cooper, A. R.; Urbinati, F.; Senadheera, S.; Zhu, A.; Liu, P. Q.; Paschon, D. E.; Zhang, L.; Rebar, E. J.; Wilber, A.; Wang, P. D.; Holmes, M. C.; Reik, A.; Hollis, R. P.; Kohn, D. B. *Blood* **2015**, *125*, 2597−2604.

(6) Fromer, M.; Pocklington, A. J.; Kavanagh, D. H.; Williams, H. J.; Dwyer, S.; Gormley, P.; Georgieva, L.; Rees, E.; Palta, P.; Ruderfer, D. M.; Carrera, N.; Humphreys, I.; Johnson, J. S.; Roussos, P.; Barker, D. D.; Banks, E.; Milanova, V.; Grant, S. G.; Hannon, E.; Rose, S. A.; Chambert, K.; Mahajan, M.; Scolnick, E. M.; Moran, J. L.; Kirov, G.; Palotie, A.; McCarroll, S. A.; Holmans, P.; Sklar, P.; Owen, M. J.; Purcell, S. M.; Donovan, M. C. *Nature* **2014**, *506*, 179−184.

(7) Fakih, M. G. *J. Clin. Oncol.* **2015**, *33*, 1809−1824.

(8) Chellapandian, D.; Lehrnbecher, T.; Phillips, B.; Fisher, B. T.; Zaoutis, T. E.; Steinbach, W. J.; Beyene, J.; Sung, L. *J. Clin. Oncol.* **2015**, *33*, 501−509.

(9) Wang, Z.; Sadovnick, A. D.; Traboulsee, A. L. L.; Ross, J. P. P.; Bernales, C. Q. Q.; Encarnacion, M.; Yee, I. M. M.; De Lemos, M.; Greenwood, T.; Lee, J. D. D.; Wright, G.; Ross, C. J.; Zhang, S.; Song, W. C.; Vilariño-Güell, C. *Neuron* **2016**, *90*, 948−954.

(10) Cutting, G. R. *Nat. Rev. Genet.* **2015**, *16*, 45−56.

(11) Bengtsson, N. E.; Hall, J. K.; Odom, G. L.; Phelps, M. P.; Andrus, C. R.; Hawkins, R. D.; Hauschka, S. D.; Chamberlain, J. R.; Chamberlain, J. S. *Nat. Commun.* **2017**, *8*, 14454.

(12) Nalls, M. A.; Pankratz, N.; Lill, C. M.; Do, C. B.; Hernandez, D. G.; Saad, M.; Destefano, A. L.; Kara, E.; Bras, J.; Sharma, M.; Schulte, C.; Keller, M. F.; Arepalli, S.; Leston, C.; Edsall, C.; Stefansson, H.; Liu, X.; Pliner, H.; Lee, J. H.; Cheng, R.; Ikram, M. A.; Ioannidis, J. P. A.; Hadjigeorgiou, G. M.; Bis, J. C.; Martinez, M.; Perlmutter, J. S.; Goate, A.; Marder, K.; Fiske, B.; Sutherland, M.; Xiromerisiou, G.; Myers, R. H.; Clark, L. N.; Stefansson, K.; Hardy, J. A.; Heutink, P.; Chen, H.; Wood, N. W.; Houlden, H.; Payami, H.; Brice, A.; Scott, W. K.; Gasser, T.; Bertram, L.; Eriksson, N.; Foroud, T.; Singleton, A. B. *Nat. Genet.* **2014**, *46*, 989−993.

(13) Yan, L.; Huang, L.; Xu, L.; Huang, J.; Ma, F.; Zhu, X.; Tang, Y.; Liu, M.; Lian, Y.; Liu, P.; Li, R.; Lu, S.; Tang, F.; Qiao, J.; Xie, X. S. *Proc. Natl. Acad. Sci. U. S. A.* **2015**, *112*, 15964−15969.

(14) Wang, K.; Gaitsch, H.; Poon, H.; Cox, N. J.; Rzhetsky. *Nat. Genet.* **2017**, *49*, 1319−1325.

(15) Albert, F. W.; Kruglyak, L. *Nat. Rev. Genet.* **2015**, *16*, 197−212.

(16) Uhlig, H. H.; Schwerd, T.; Koletzko, S.; Shah, N.; Kammermeier, J.; Elkadri, A.; Ouahed, J.; Wilson, D. C.; Travis, S. P.; Turner, D.; Klein, C.; Snapper, S. B.; Muise, A. M. *Gastroenterology* **2014**, *147*, 990−1007.

(17) Zhang, M.; Xi, Z.; Zinman, L.; Bruni, A. C.; Maletta, R. G.; Curcio, S. A. M.; Rainero, I.; Rubino, E.; Pinessi, L.; Nacmias, B.; Sorbi, S.; Galimberti, D.; Lang, A. E.; Fox, S.; Surace, E. I.; Ghani, M.; Guo, J.; Sato, C.; Moreno, D.; Liang, Y.; Keith, J.; Traynor, B. J.; St. George-Hyslop, P.; Rogaeva, E. *Brain* **2015**, *138*, e380.

(18) Wapinski, O.; Chang, H. Y. *Trends Cell Biol.* **2011**, *21*, 354−361.

(19) Oftedal, B. E.; Hellesen, A.; Erichsen, M. M.; Bratland, E.; Vardi, A.; Perheentupa, J.; Kemp, E. H.; Fiskerstrand, T.; Viken, M. K.; Weetman, A. P.; Fleishman, S. J.; Banka, S.; Newman, W. G.; Sewell, W. A. C.; Sozaeva, L. S.; Zayats, T.; Haugarvoll, K.; Orlova, E. M.; Haavik, J.; Johansson, S.; Knappskog, P. M.; Lovas, K.; Wolff, A. S. B.; Abramson, J.; Huesbye, E. S. *Immunity* **2015**, *42*, 1185−1196.

(20) Forbes, S. A.; Beare, D.; Boutselakis, H.; Bamford, S.; Bindal, N.; Tate, J.; Cole, C. G.; Ward, S.; Dawson, E.; Ponting, L.; Stefancsik, R.; Harsha, B.; YinKok, C.; Jia, M.; Jubb, H.; Sondka, Z.; Thompson, S.; De, T.; Campbell, P. J. *Nucleic Acids Res.* **2017**, *45*, D777−D783.

(21) Baaske, M. D.; Foreman, M. R.; Vollmer, F. *Nat. Nanotechnol.* **2014**, *9*, 933−939.

(22) Lin, M.; Song, P.; Zhou, G.; Zuo, X.; Aldalbahi, A.; Lou, X.; Shi, J.; Fan, C. *Nat. Protoc.* **2016**, *11*, 1244−1263.

(23) Xu, J. J.; Zhao, W. W.; Song, S.; Fan, C.; Chen, H. Y. *Chem. Soc. Rev.* **2014**, *43*, 1601−1611.

(24) Scognamiglio, V.; Antonacci, A.; Lambreva, M. D.; Litescu, S. C.; Rea, G. *Biosens. Bioelectron.* **2015**, *74*, 1076−1086.

DOI: 10.1021/acs.analchem.9b01841
Anal. Chem. 2019, 91, 10016−10025

(25) Courbet, A.; Endy, D.; Renard, E.; Molina, F.; Bonnet, J. *Sci. Transl. Med.* **2015**, *7*, 289ra83.
(26) Limaj, O.; Etezadi, D.; Wittenberg, N. J.; Rodrigo, D.; Yoo, D.; Oh, S. H.; Altug, H. *Nano Lett.* **2016**, *16*, 1502−1508.
(27) Zhang, H.; Wang, Y.; Zhao, D.; Zeng, D.; Xia, J.; Aldalbahi, A.; Wang, C.; San, L.; Fan, C.; Zuo, X.; Mi, X. *ACS Appl. Mater. Interfaces* **2015**, *7*, 16152−16156.
(28) Reina, G.; González-Domínguez, J. M.; Criado, A.; Vázquez, E.; Bianco, A.; Prato, M. *Chem. Soc. Rev.* **2017**, *46*, 4400−4416.
(29) Oliveira, O. N.; Iost, R. M.; Siqueira, J. R.; Crespilho, F. N.; Caseli, L. *ACS Appl. Mater. Interfaces* **2014**, *6*, 14745−14766.
(30) Jang, M.; Kim, H.; Lee, S.; Kim, H. W.; Khedkar, J. K.; Rhee, Y. M.; Hwang, I.; Kim, K.; Oh, J. H. *Adv. Funct. Mater.* **2015**, *25*, 4882−4888.
(31) Castillo Diaz, L. A.; Elsawy, M.; Saiani, A.; Gough, J. E.; Miller, A. F. *J. Tissue Eng.* **2016**, *7*, 1−15.
(32) Koh, W. G.; Revzin, A.; Pishko, M. V. *Langmuir* **2002**, *18*, 2459−2462.
(33) Nagahama, K.; Kimura, Y.; Takemoto, A. *Nat. Commun.* **2018**, *9*, 2195−2206.
(34) Sukul, P. K.; Bose, P.; Takei, T.; Yaghi, O. M.; He, Y.; Lee, M.; Tashiro, K. A. *Chem. Commun.* **2016**, *52*, 1579−1581.
(35) King, P. J. S.; Saiani, A.; Bichenkova, E. V.; Miller, A. F. A *Chem. Commun.* **2016**, *52*, 6697−6700.
(36) Culver, H. R.; Clegg, J. R.; Peppas, N. A. *Acc. Chem. Res.* **2017**, *50*, 170−178.
(37) Wang, D.; Hu, Y.; Liu, P.; Luo, D. *Acc. Chem. Res.* **2017**, *50*, 733−739.
(38) Pianowski, Z. L.; Karcher, J.; Schneider, K. *Chem. Commun.* **2016**, *52*, 3143−3146.
(39) Armbruster, D. A.; Pry, T. *Clin. Biochem. Rev.* **2008**, *29*, 49−52.
(40) Moore, D. S. *Biochem. Educ.* **1985**, *13*, 10−11.
(41) King, P. J. S.; Giovanna Lizio, M.; Booth, A.; Collins, R. F.; Gough, J. E.; Miller, A. F.; Webb, S. J. *Soft Matter* **2016**, *12*, 1915−1923.

DOI: 10.1021/acs.analchem.9b01841
Anal. Chem. 2019, 91, 10016−10025